On a Spacetime-Lens Principle which suggests a positive curvature of the universe

Michal Křížek[1]
Institute of Mathematics, Czech Academy of Sciences, Žitná 25, 115 67 Prague 1, Czech Republic
krizek@math.cas.cz

(Submitted on 12.08.2024; Accepted on 13.01.2025)

Abstract. According to infrared measurements of the James Webb Space Telescope, there exist very luminous galaxies at distances $z \sim 13$ that should not exist according to the standard ΛCDM cosmological model for the flat universe with normalized curvature index $k = 0$. In this paper, we introduce a spacetime-lens principle that could explain why these very distant galaxies shine so much. We present 10 specific examples showing that the observed large flux luminosities may be mere optical effects due to the positive curvature index $k = 1$ of an expanding 3-sphere modeling our physical universe in time. For Euclidean or hyperbolic geometries such large flux luminosities seem implausible. This suggests that the right model of a homogeneous and isotropic physical universe for each fixed time instant is a 3-sphere. The angular size of the most frequent fluctuations in the power spectrum of the CMB radiation is about 1°. This enables us to exclude flat and hyperbolic geometries and also indicates that the correct curvature index is $k = 1$.

Key words: luminosity distance; comoving distance; supermassive black hole, cosmic microwave background; maximally symmetric manifold

1. Introduction

For the time being we do not know what is the global geometry of our universe, if it is spherical, flat, or hyperbolic, see e.g. Carroll (2014), Chiba and Nakamure (1998), Křížek (2024), Peebles (1993), Suntola (2018), Weinberg (1972). The James Webb Space Telescope recently found very distant and luminous galaxies whose masses are estimated up to 10^{11} stars at the distance ~ 13 Gly, see Wang (2023) (and also Labbe et al. (2023), Laporte et al. (2021)). Such large galaxies with so many stars should not exist according to the standard ΛCDM cosmological model of a currently proposed flat universe. In this paper, we show that these large flux luminosities could be explained by a positive curvature of our universe that creates several fairly big artificial optical magnification effects (see Examples 1–3 below). We focus on a geometrical approach which is more illustrative and pedagogically more valuable than mere manipulations with arithmetic formulas.

Karl Schwarzschild (1900) conjectured that our universe can roughly be described by a huge three-dimensional sphere (called 3-*sphere*) in the Euclidean space $\mathbb{E}^4$,

$$\mathbb{S}^3_a = \{(x, y, z, w) \in \mathbb{E}^4 \,|\, x^2 + y^2 + z^2 + w^2 = a^2\}, \tag{1}$$

where $a > 0$ is its radius and the *curvature* $1/a$ of $\mathbb{S}^3_a$ is positive. Also Albert Einstein (1917, p. 152) in his famous paper on cosmology assumes that the entire universe can be modeled by the sphere $\mathbb{S}^3_a$ with fixed a. In this way he could avoid initial and boundary conditions for his field equations. If $a = 1$ we write only $\mathbb{S}^3$. Let us point out that ten different ways to imagine the unit 3-sphere $\mathbb{S}^3$ are described in Křížek and Somer (2023, Sect. 6.2).

Alexander Friedmann (1922) applied Einstein's field equations to the entire universe. In this way he obtained an ordinary differential equation for the time variable radius $a = a(t)$. This equation (cf. (23) below) is at present called the Friedmann equation and it is the basis of the current ΛCDM cosmological model. In another paper Friedmann (1924) considers a negative curvature index $k = -1$. However, he suggests that only negative mass density is possible for a static universe (see Friedmann (1924, p. 2006)) and thus it is not clear how to satisfy such a paradoxical requirement. Note also that Friedmann did not consider the case $k = 0$, which corresponds to the three-dimensional Euclidean space $\mathbb{E}^3$ now favored by the ΛCDM model. We show that there is a very big difference of observed galaxies between the cases $k = 0$ and $k = 1$ for large redshifts.

For $k = 1$ our approach is more general than that described by the ΛCDM model, since the radius $a = a(t)$ may not satisfy the Friedmann equation (23). It can be any positive continuous function, which thus serves as a pedagogical tool to understand the geometrical properties of spherical spacetime, regardless of general relativity.

Using movements of globular clusters, Schwarzschild (1900) derived for the spherical model (1) that the corresponding radius a should be at least 10^8 au $\approx 1.5 \cdot 10^{19}$ m. At present, this lower bound can be made much larger. We know that the mean density of the universe in our neighborhood is $\rho \approx 10^{-26}$ kg/m^3, i.e., approximately 6 protons per cubic meter. Moreover, over 10^{12} galaxies are currently observed each having on average about 10^{11} stars. Consequently, the total mass M of the entire universe can be roughly bounded from below by $M > 10^{12} \cdot 10^{11} \cdot M_\odot = 2 \cdot 10^{53}$ kg. Since the volume of 3-sphere is $V = 2\pi^2 a^3 = M/\rho$, we find that $\pi^2 a^3 > 10^{53+26}$ m^3. Hence, for the present value of the radius we get the following lower bound

$$a > \sqrt[3]{10^{78}} = 10^{26} \text{ [m]}. \tag{2}$$

Furthermore, let L be the intrinsic bolometric luminosity of a galaxy (i.e., the total luminosity integrated over all frequencies and measured in Watts). The *luminosity distance* d_{L} is related to the flux ℓ measured in W/m^2 by (see Weinberg (1972, p. 421))

$$\ell = \frac{L}{4\pi d_{\mathrm{L}}^2}, \quad \text{i.e.} \quad d_{\mathrm{L}} = \sqrt{\frac{L}{4\pi \ell}}. \tag{3}$$

For a geometrical interpretation of this distance we recall that it is practically equal to the Euclidean distance in a close neighborhood of the Milky Way. However, for distant objects we have to take into account that the universe expands and might be curved. The luminosity distance for the 3-sphere will be defined later in (9).

Further, let us note that the luminosity distance in Mpc is usually calculated from the observed apparent magnitude μ and the absolute magnitude μ_{abs} of a given galaxy by the Pogson's equation $\mu - \mu_{\mathrm{abs}} = 25 + 5 \log_{10} d_{\mathrm{L}}$. This is a key relation in cosmology, because we can use the observed flux to obtain d_{L}, see e.g Carroll et al. (1992), Křížek et al. (2015, p. 110), Weinberg (1972).

To introduce the main idea of the spacetime-lens principle, we initially assume that the radius a in (1) is a fixed constant. Note that this assumption is satisfied for the well-known Einstein's static universe. For clarity, consider only the cross section of the 3-sphere (1) by the equatorial hyperplane $w = 0$. Suppose that the corresponding 2-sphere $\mathbb{S}^2_a$ is perfectly transparent. Let an observer be located at an arbitrary point N of the 2-sphere $\mathbb{S}^2_a$. Without loss of generality we may assume that it is at the North Pole of the spherical coordinate system (see Figure 1), since 2-sphere is a maximally symmetric manifold. Note that this is not the North Pole of the celestial sphere.

Furthermore, suppose there are two galaxies of the same size and the same bolometric luminosity. For simplicity, we assume that they are disc galaxies (spiral or lenticular) and that they are oriented facing an observer. In this case their observed flux intensity is proportional to the square of their diameter. Then the observer will see these two galaxies at the same angular size φ and also possessing the same flux even though their physical distances to N are radically different. This means that the observed flux intensity does not decrease with square of the distance like in Euclidean space. Only in a close neighborhood of the North Pole N, where the space is locally almost flat, the observed flux decreases approximately with the square of the distance (see Figure 2).

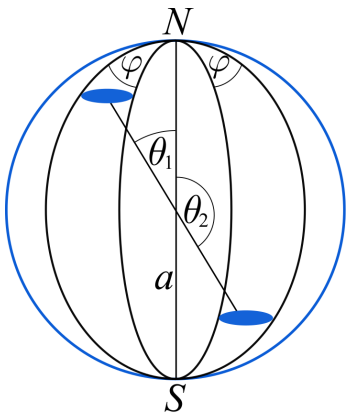

Fig. 1. Two galaxies having the same diameter and the same bolometric luminosity are seen from the North Pole N of the sphere $\mathbb{S}^2_a$ under the same angle φ when the radius a is fixed. Their observed flux will also be the same although their distances along geodesics to N measured through spherical coordinates θ_1 and θ_2 differ substantially.

Example 1. Assume that the spherical-coordinate angle of the upper galaxy is $\theta_1 = 30°$ and that of the lower galaxy is $\theta_2 = 180° - \theta_1 = 150°$, see Figure 1. Then their viewing angle φ from N is the same (proportional to $1/\sin\theta_1 = 1/\sin\theta_2$) and the lower galaxy is 5 times more distant from N than the upper galaxy. The observer registers the corresponding photons traveling along geodesics (i.e. great circles) passing through the North Pole N. Since he sees both the galaxies under the same viewing angle φ, the same observed

flux intensity must be detected. (In Euclidean space, the closer galaxy would have a diameter 5 times larger and would be 25 times brighter than the more distant one.)

For $\theta_1 = 15^\circ$ and $\theta_2 = 180^\circ - \theta_1 = 165^\circ$, the distance of the lower galaxy from N would be even 11 times larger than that of the upper galaxy. It means that distant objects near the South Pole S (the antipodal point to N, see Křížek and Somer (2023, p. 167) and Suntola (2018, p. 277)) will be extremely magnified and their observed apparent luminosity will be enormous. This is not a coordinate effect but a real physical effect, cf. also specific Examples 2–5, 9, and 10 below.

Further, recall that a *three-dimensional manifold* is a set of points for which there exists an open neighborhood that can be continuously mapped onto an open set in $\mathbb{E}^3$ such that the inverse is continuous, too. If this mapping is smooth, then the manifold is called *smooth* and looks locally as Euclidean space. However, locally flat does not imply that it is globally flat.

According to the *Copernican principle*, our Earth is not at some privileged part of the physical universe. According to the *Einstein cosmological principle*, the universe on each isochrone is homogeneous and isotropic on large scales. These principles are, in fact, assumptions. By Weinberg (1972, Chapt. 13) and Penrose (2005, p. 721) there exists exactly three maximally symmetric three-dimensional manifolds up to scaling, namely $\mathbb{S}^3$, $\mathbb{E}^3$, and the hyperbolic pseudosphere $\mathbb{H}^3$ that perfectly model the required homogeneity and isotropy. Their corresponding curvature indices are $k = 1, 0, -1$, respectively. We shall see that the luminosity distance, angular distance, and comoving distance essentially depend on a particular choice of k when the cosmological redshift z is large.

In the next section, we introduce the space-lens principle for the 3-sphere with time independent radius to illustrate the basic ideas. In Section 3, we show how it can be modified for an expanding 3-sphere (1) to the spacetime-lens principle which covers also the standard FLRW metric, see (30) below. This principle can explain the observed large flux intensities of galaxies at $z \gtrsim 13$ if $k = 1$. In Section 4, we present the main theorem stating that the trajectory of a photon in a linearly expanding space is a logarithmic spiral when $k = 1$. This enables us to estimate the comoving distance θ by means of the measured cosmological redshift z. In this paper, we will carefully distinguish between the coordinate z in (1) and redshift z to avoid ambiguities. Several arguments against Euclidean ($k = 0$) and hyperbolic ($k = -1$) models of the physical universe are collected in Section 5. The last Section 6 contains a few concluding remarks.

2. The space-lens principle for a non-expanding 3-sphere

The angular size α of galaxies (except for the Milky Way) is indirectly proportional to their distance if the space is modeled by Euclidean space $\mathbb{E}^3$ (keeping in mind that $\sin\alpha \approx \tan\alpha \approx \alpha$ for small α measured in radians). In this case, the areal size (measured in steradians) and thus also observed flux intensities of galaxies decrease with the square of their distance, assuming the universe is perfectly transparent.

However, these dependencies are completely different for the 3-sphere. To see this we set

$$\theta = \frac{d}{a}, \tag{4}$$

where θ is called the *comoving distance*, a is the radius of the 3-sphere (1), and d is the usual physical distance along geodesics, see Figure 1.

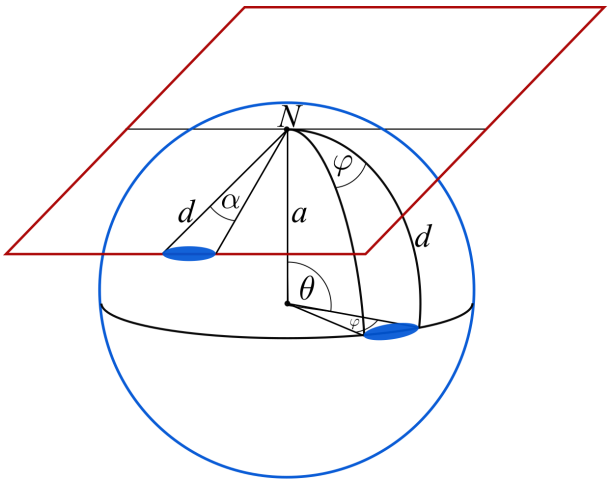

Fig. 2. According to (5), the angular size α of a galaxy in $\mathbb{E}^2$ is always smaller than if this galaxy were at the same distance $d > 0$ from N on the sphere $\mathbb{S}^2_a$ with angular size φ.

Example 2. Consider two galaxies in $\mathbb{E}^2$ and $\mathbb{S}^2_a$ having the same diameter $D > 0$, the same bolometric luminosity, and the same distance d from the point N. We see that $d = a\theta$ for $k = 1$, see Figure 2. Then the corresponding angular size $\alpha = D/d$ for $k = 0$ is always smaller than the angular size φ for $k = 1$; namely, by (4) we have

$$\alpha = \frac{D}{d} = \frac{D}{a\theta} < \frac{D}{a \sin\theta} = \varphi \tag{5}$$

for $\theta \in (0, \pi)$. This represents another artificial magnification effect which is different from that sketched in Figure 1. By (4) and (5) we find that

$$\frac{\varphi}{\alpha} = \frac{\theta}{\sin\theta}\,.$$

Consequently, if the comoving distance is for instance $\theta = \pi/2$, then the ratio between the two agular sizes is equal to $\varphi/\alpha = \pi/2 \doteq 1.57$.

Figure 3 illustrates a typical dependence (up to a multiplicative constant D/a) of the angular size of a reference galaxy on the dimensionless comoving

distance $\theta \in (0, \pi)$ on each of the maximally symmetric manifolds when $k = 1, 0, -1$ and $a = 1$. This is not taken into account in Pilipenko (2013) and many cosmological calculators. The observed flux intensities are proportional to the square of angular sizes. Hence, for $\theta \in (0, \pi)$ we set

$$R(\theta) = \frac{\theta^2}{\sin^2 \theta} \tag{6}$$

and thus, the magnification effect for flux intensities is much larger on $\mathbb{S}^3$ than on $\mathbb{E}^3$ when $\theta \in (0, \pi)$ is large, see Table 1 and Figures 2 and 4. For instance, if the comoving distance is again $\theta = \pi/2$, then $R(\theta) = \pi^2/4 \doteq 2.467$. Consequently, the ratio $R(\theta)$ between the flux in $\mathbb{S}^3$ is almost 2.5 times higher than that in $\mathbb{E}^3$ for a given reference galaxy.

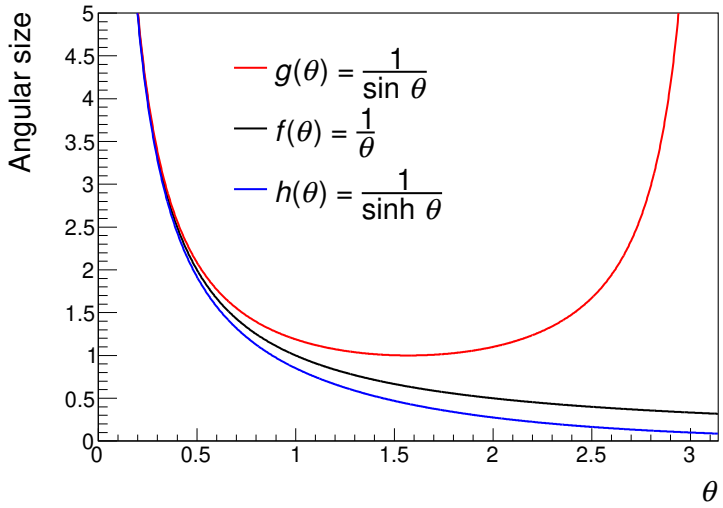

Fig. 3. The angular size of a given reference galaxy depends quite differently (up to some multiplicative factor) on the comoving distance $\theta \in (0, \pi)$ on each of the manifolds $\mathbb{S}^3$, $\mathbb{E}^3$, and $\mathbb{H}^3$.

The graph in Figure 4 leads the following paradoxical example on the 3-sphere $\mathbb{S}^3$ that is based on special properties of the function $\theta \in (0, \pi) \mapsto \theta/\sin\theta$ and its square.

Example 1 (continuation). Consider two galaxies as in Figure 1. Let the upper galaxy at $\theta_1 = 30°$ has a twice larger diameter than the lower one at $\theta_2 = 170°$ and let the ratio of their absolute luminosities is $2^2 = 4$. However, the observer at N will see that the lower galaxy produces a larger flux intensity than the upper one, even though the lower galaxy is twice smaller in diameter

θ	$R(\theta)$
30°	1.097
60°	1.462
90°	2.467
120°	5.848
150°	27.416
180°	∞

Table 1. The ratio $R(\theta) = \theta^2/\sin^2\theta$ between flux intensities of a given reference galaxy for the manifolds $\mathbb{S}^3$ and $\mathbb{E}^3$ for several values of θ.

and much more distant from N than the upper galaxy. The reason is that

$$16 = \frac{4}{\sin^2\theta_1} < \frac{1}{\sin^2\theta_2} = 33.163,$$

i.e., the twice smaller galaxy in diameter produces more than twice larger observed flux although it is at least 5 times more distant from N than the larger galaxy.

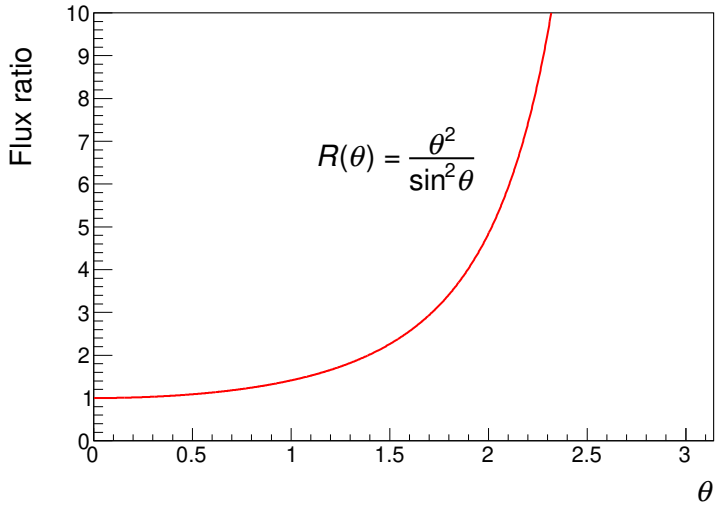

Fig. 4. The ratio $R(\theta)$ between flux intensities of a given reference galaxy for the manifolds $\mathbb{S}^3$ and $\mathbb{E}^3$ is large if the comoving distance θ is also large: $0 \ll \theta < \pi$.

The above-described two nonlinear optical magnification effects from Examples 1 and 2 lead to the so-called *space-lens principle*. It is because converging geodesics passing through the North Pole N resemble the bending of

light rays in a converging lens. This bending effect works along their entire trajectories, cf. Figures 1 and 2. Note that geodesics in hyperbolic geometries resemble functioning of a diverging lens.

3. The spacetime-lens principle for an expanding 3-sphere

The term "universe" is used in cosmology with various meanings: true spacetime, true space (i.e. a part of spacetime at a fixed time instant), and the observable universe, which is seen as a projection on the celestial sphere. These are three different objects. Their mathematical models are also three completely different manifolds (see Figure 5).

In this section, we describe the third apparent magnification effect caused by the expansion of the 3-sphere in time. First, let us realize that the 3-sphere cannot change its geometry during its continual evolution, see Figure 5, i.e., the spherical model with bounded manifold $\mathbb{S}^3_a$ cannot be continuously deformed into the Euclidean or hyperbolic model. From now on assume that $a = a(t) > 0$ is an increasing differentiable function describing the radius of the expanding 3-sphere (1). It is called the *expansion function* and for the time being it does not have to satisfy the well-known Friedmann equation.

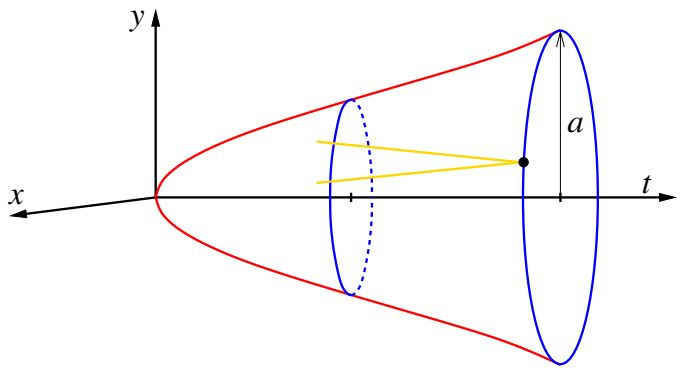

Fig. 5. Schematic illustration of three different manifolds that are used to model our physical universe for $k = 1$. For simplicity, the number three of space dimensions is reduced to one. Thus, the 3-sphere (1) with radius $a = a(t) > 0$ at a fixed time instant t is replaced only by its great (blue) circle $\mathbb{S}^1_a$ for $z = w = 0$. This model expresses the homogeneity and isotropy of the universe. The model of spacetime can be obtained by rotation of the (red) graph of the expansion function $a = a(t)$ about the time axis t. The observable universe is marked by the (yellow) manifold given by the past light cone whose vertex corresponds to an observer. This cone is deformed towards the origin of coordinates, see Figure 6 and also Davis and Lineweaver (2004), The last two models (red and yellow) do not satisfy the homogeneity required by the Einstein cosmological principle.

Recall that the *redshift* of a galaxy resulting from its radial motion is defined by

$$z = \frac{\lambda_0}{\lambda_1} - 1,$$

where λ_0 is the observed wavelength of a particular spectral line and λ_1 the corresponding emitted wavelength. For the associated radii of $\mathbb{S}^3_a$ we have by Carroll et al. (1992) and Peebles (1993) that

$$\frac{a(t_0)}{a(t_1)} = \frac{\lambda_0}{\lambda_1} = z + 1. \tag{7}$$

Here t_1 is the time instant when a photon was emitted and t_0 when it was received, i.e. $0 < t_1 < t_0$ and

$$t_0 \approx 13.8 \text{ Gyr} \tag{8}$$

is an approximate *age of the universe*.

The *luminosity distance* for the 3-sphere is given by the following formula, see e.g. Mészáros et al. (2011, Eqs. (1)–(3)),

$$d_{\mathrm{L}} = a(t_0)(z+1)\sin\theta. \tag{9}$$

Therefore, for the measured flux ℓ we obtain by (3) that (cf. Weinberg (1972))

$$\ell = \frac{L}{4\pi a^2(t_0)(z+1)^2\sin^2\theta}.$$

Here one factor $(z+1)$ appears in the denominator, since photons loose their energy during the expansion of the physical universe. The second factor $(z+1)$ in this denominator is due to the fact that 1 second lasted longer when a photon was emitted than when it was received.

Note that for any $k = 1, 0, -1$, we have (see e.g. Peebles (1993, pp. 313, 328))

$$\ell = \frac{L}{4\pi a^2(t_0)(z+1)^2\operatorname{sinn}^2\theta},$$

where sinn depends on the curvature index k as follows (see Figure 3)

$$\operatorname{sinn}\theta = \begin{cases} \sin\theta & \text{if } k = 1, \\ \theta & \text{if } k = 0, \\ \sinh\theta & \text{if } k = -1. \end{cases} \tag{10}$$

We see that the two galaxies from Figure 1 have, paradoxically, according to (9) the same luminosity distance from N for a non-expanding universe with redshift $z = 0$. So there is a serious ambiguity (non-uniqueness) in establishing the correct comoving distance $\theta \in (0, \pi/2] \cup (\pi/2, \pi]$, i.e., if an object is above or below the equatorial hyperplane $w = 0$, cf. (1). We see that the *angular distance*, defined by (see Weinberg (1972, p. 423))

$$d_{\mathrm{A}}(z) = \frac{d_{\mathrm{L}}(z)}{(z+1)^2},$$

possesses the same non-uniqueness problem, and thus it also does not help us to verify whether

$$\theta \in (0, \pi/2] \qquad \text{or} \qquad \theta \in (\pi/2, \pi]. \tag{11}$$

Therefore, in Section 4, we show how to find a proper comoving distance θ from the observed cosmological redshift z.

An increasing radius of the 3-sphere produces the third apparent magnification effect which is called the *time-lens principle*, see Křížek (1999), Křížek et al. (2015, p. 314). So now we show how the intrinsic expansion of the universe with $k = 1$ apparently magnifies the angular size of very distant objects, see also Pilipenko (2013) for $k = 0$. It practically functions at very "large" distances — at least several billion light years. On the other hand, this apparent magnification effect at "short" distances is almost negligible.

We see very distant galaxies with large time delay given by the finite speed of light. Hence, we must consistently distinguish between "at that time" and "actual dimensions", i.e., the size of the universe when observed photons left a particular galaxy and the universe was much smaller, and "today's" dimensions when "ancient" photons (see the yellow lines in Figures 5 and 6) arrived at our ground-based telescopes. Roughly speaking, the younger the objects which are observed, the larger the magnification appears. Therefore, by angular measurements we paradoxically see a very distant object as being larger. From (7) we find that this angular magnification is proportional to $z + 1$. This partly explains the "observed" superluminal speeds of plasma jets at distant quasars, see e.g. Pearson and Zensus (1987, p. 3). Some ejections achieved speeds far exceeding the speed of light. Moreover, according to (5), the absolute length D of these jets should be $\theta/\sin\theta$ times shorter when we replace $k = 0$ by $k = 1$. For another reason see also Křížek et al. (2015, p. 309).

Let us illustrate supporting evidence of the functioning of the time-lens principle by another two examples.

Example 3. The cosmic microwave background (CMB) radiation as observed by the Planck Collaboration (2014) comes from the period

$$t_2 = 380\,000 \text{ years} \tag{12}$$

after the Big Bang, when atoms were created and the universe started to be transparent for photons (cf. also Vavryčuk (2018)). This almost homogeneous and almost isotropic radiation corresponding to the temperature 2.73 K comes from all directions of the sky at the distance of about 13.8 Gly — the so-called *horizon of the observable universe*. According to Eisenstein and Bennett (2008), the corresponding redshift is about

$$z = 1089. \tag{13}$$

Thus the CMB came into existence in the period when the universe was approximately 1000 times smaller in diameter than is at present. In other words, every current cubic meter of space was concentrated on average in one cubic millimeter at that time.

It would be a mistake to believe that the well-known map of the CMB shows the entire universe, how it looked like 380 000 years after the Big Bang. This

map only shows only a part of the observable universe, which is a relatively very small two-dimensional slice $\mathbb{S}^2_r$ with radius $r = a(t_2)$ of the three-dimensional manifold $\mathbb{S}^3_{a(t_2)}$ corresponding to the universe with $z \approx 1089$, see Figure 5. For instance, the ball region of all galaxies with $z \lesssim 13$ is not contained in this slice. All known galaxies such as M31, M51, M87, ... are in this region (each map of CMB currently observed from these galaxies would look different than that from Earth).

Let us emphasize that the observable universe is not homogeneous, since for different cosmological redshifts z, it has a different mass density. Thus, it is an entirely different object than the universe as a space. From a similar reason the spacetime is also not homogeneous. Therefore, the expansion of the universe is a completely different notion than the expansion of the observable universe.

Hence, when the CMB radiation was created, the universe would be represented in Figure 5 by an extremely small circle (near the origin) with radius ca. 1090 times smaller than the radius $a(t_0)$ of the circle corresponding to the present time. Consequently, astronomers observe the sphere $\mathbb{S}^2_r$ with CMB extremely magnified (cf. also Figure 6). Moreover, from (7) and (2) we get the following lower bound

$$a(t_2) = \frac{a(t_0)}{z+1} > \frac{10^{26}}{1090}\ \mathrm{m} \approx 3\ \mathrm{Mpc} \approx 9\ \mathrm{Mly}. \tag{14}$$

Furthermore, we will estimate the behavior of the expansion function $a = a(t)$ in a neighborhood of the time instant t_2 corresponding to the origin of CMB. Using (7), (8), (12), and (13), we get

$$\frac{a(t_2)}{t_2} = \frac{t_0}{(z+1)t_2}\frac{a(t_0)}{t_0} = \frac{13.8 \cdot 10^9}{1090 \cdot 380\,000}\frac{a(t_0)}{t_0} = 33.3 \cdot \frac{a(t_0)}{t_0}, \tag{15}$$

and thus the mean expansion rate of the space on the interval $(0, t_2)$ was 33.3 times larger than that on the interval $(0, t_0)$. Taking into account that 1 yr $\approx \pi 10^7$ s, we find from (2) and (15) that

$$\frac{a(t_2)}{t_2} > 33.3\frac{10^{26}}{13.8 \cdot 10^9 \cdot \pi \cdot 10^7}\ \mathrm{m/s} \doteq 25\,c, \tag{16}$$

where c is the speed of light in a vacuum. Note that such a large expansion rate does not contradict to the special theory of relativity, see e.g. Davis and Lineweaver (2004). The inequality (16) indicates that the expansion function had much bigger the first time derivative $\dot{a} = \dot{a}(t)$ over the interval $(0, t_2)$ than at present (see Figure 5). The expansion speed, given by the *Hubble parameter*

$$H(t) = \frac{\dot{a}(t)}{a(t)}, \tag{17}$$

was very large at that time. Recall that the present measured value of the Hubble-Lemaître constant is

$$H_0 = H(t_0) = \frac{\dot{a}(t_0)}{a(t_0)} \approx 70\ \mathrm{km\,s^{-1}Mpc^{-1}} \approx 2.27 \cdot 10^{-18}\ \mathrm{s^{-1}}. \tag{18}$$

Further analysis of the CMB radiation is given in Example 10.

Example 4. An enormous magnification is produced the Big Bang itself, which appeared roughly 13.8 Gyr ago, see (8). Although it happened in a minimal volume, see Křížek and Somer (2023, p. 117), its present position seems to be on the possibly greatest 2-sphere (the so-called *horizon*) with an unimaginable large radius (much larger than in the previous example).

Thus, the farther we look, the corresponding sphere seems to be bigger and bigger, even though the universe was smaller and smaller. This is the main reason of functioning of the time-lens principle. Monitored objects from the time t are seemingly magnified $a(t_0)/a(t)$-times and thus the magnification effect is "small" close to N, see Weinberg (1972, p. 423). The magnification effects described in Sections 1, 2, and 3 lead to the so-called *spacetime-lens principle*.

4. The main theorem

Now we show how to estimate the comoving distance θ corresponding to a given cosmological redshift z. Throughout this section we assume that $k = 1$ and that the expansion function $a = a(t)$ is linear over some long time interval (t_1, t_0), where t_0 is given by (8). This assumption is not too restrictive (see Křížek (2024)), since the actual expansion function is almost linear during the last 12 Gyr, see also the situation sketched in Figure 7 below, which illustrates the behavior of $a = a(t)$ for the standard cosmological FLRW model driven by the Friedmann equation.

Theorem 1. *Let $\mathbb{S}^3_a$ expand at a constant velocity $V > 0$ over an interval (t_1, t_0), i.e., $\dot{a}(t) = V$ for all $t \in (t_1, t_0)$. Then the trajectory of a photon towards the observer at N can be described by a logarithmic spiral (in space variables) with slope angle $\phi = \arctan(c/V)$ and the comoving distance*

$$\theta = (\tan\phi)\ln(z+1) = \frac{c}{V}\ln(z+1)$$

corresponds to the cosmological redshift $z \geq 0$.

P r o o f. Each geodesic of $\mathbb{S}^3_{a(t)}$ is represented by an expanding great circle which lies in a plane passing through the center of $\mathbb{S}^3_{a(t)}$. Thus since a photon traveling to N moves along geodesics in a plane, we can choose without loss of generality the Cartesian coordinate system in (1) so that $w = z = 0$. Since the space expands in the radial direction in this plane at the constant velocity V and since the photon moves in the tangential direction at the constant velocity c, the total velocity $\sqrt{c^2 + V^2}$ is also constant and thus the corresponding slope angle

$$\phi = \arctan\frac{c}{V}$$

is constant, too, see Figure 6. Therefore, the trajectory of the photon is described by the logarithmic spiral in the standard polar coordinates (r, θ) as follows:

$$r(\theta) = a_1 \exp(\theta \operatorname{cotan}\phi), \tag{19}$$

where $a_1 = a(t_1) > 0$ and $\phi > 0$ are given constants.

From (19) and (7) we find the searched relation between z and θ,

$$\theta = \frac{1}{\operatorname{cotan}\phi} \ln \frac{a_0}{a_1} = (\tan\phi) \ln(z+1) = \frac{c}{V} \ln(z+1), \tag{20}$$

where $a_0 = a(t_0)$, see Table 2. □

θ	z
0°	0
30°	0.69
60°	1.85
90°	3.81
120°	7.12
150°	12.71

Table 2. Redshifts corresponding to several comoving distances θ given by (20) for the 3-sphere and $V = c$.

From (18) and (2) we get the following lower bound

$$\dot{a}(t_0) = H_0 a(t_0) > 2.27 \cdot 10^{-18}\ \mathrm{s}^{-1} \cdot 10^{26}\ \mathrm{m} = 2.27 \cdot 10^{8}\ \mathrm{m/s}.$$

Since the estimate (2) is indeed very rough, we shall assume for simplicity in the next two examples that the present expansion speed $V = \dot{a}(t)$ is equal to the speed of light.

Example 5. So let $V = c$ and consider a galaxy with redshift $z = 13$, see Wang et al. (2023). (As of 2024 the most distant known galaxy JADES-GS-z14-0 has even $z = 14.32$.) From the relation $\tan\phi = c/V$ we find that the slope angle is $\phi = 45°$, see Figure 6. In fact, this figure represents the orthogonal projection of Figure 5 along the time axis. Using (7), we get

$$14 a_1 = a_0 \tag{21}$$

(i.e., the volume of $\mathbb{S}^3_{a_1}$ is $14^3 = 2744$ times smaller than the present volume of $\mathbb{S}^3_{a_0}$). According to (20),

$$\theta \approx \ln 14 = 2.639 > \frac{\pi}{2}$$

and thus the galaxy with $z = 13$ is below the equatorial hyperplane $w = 0$ and $\theta = 2.639$ rad $= 151.2°$, cf. Table 2. From (6) we see that the flux ratio

$$R(\theta) = 30.02 \tag{22}$$

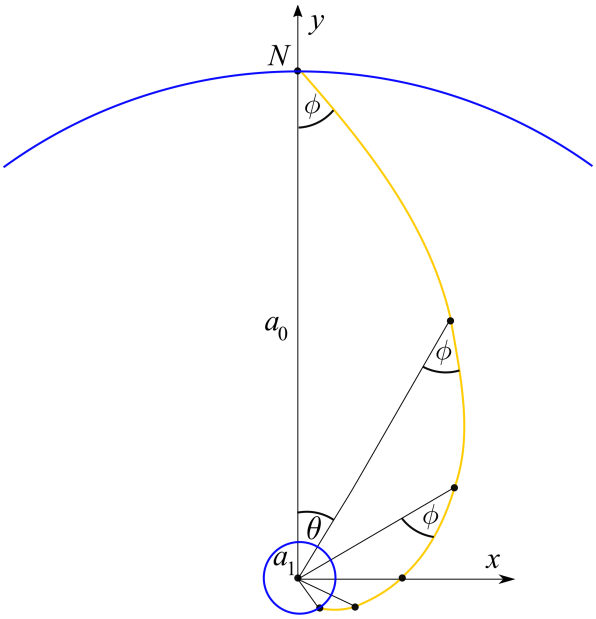

Fig. 6. The curved (yellow) trajectory of a photon in a linearly expanding universe modeled by the (blue) sphere $\mathbb{S}^3_{a(t)}$ in the plane $z = w = 0$. It is described by the logarithmic spiral (19) whose slope angle $\phi = \arctan(c/V)$ is constant. Redshifts corresponding to comoving distances θ for the slope angle $\phi = 45^\circ$ are given in Table 2, see also Suntola (2018, p. 253).

is really very large, cf. Figure 4. This explains why some very distant galaxies and quasars seem to be so luminous if we would assume that $k = 0$. Therefore, the actual bolometric luminosities of these objects for $k = 1$ are at least one order of magnitude smaller than absolute luminosities calculated from flux measurements. We will call $R(\theta)$ the *reduction factor*. It actually states by how much is the mass calculated from the luminosity smaller when we change $k = 0$ by $k = 1$.

It is well known that the length of the logarithmic spiral is equal to

$$s(\theta_0, \theta_1) = \frac{r(\theta_0) - r(\theta_1)}{\cos\phi},$$

where $\phi \in (0, \pi/2)$ and $0 \leq \theta_0 \leq \theta_1$. Hence, for $V = c$ we get by (21) that

$$s = \frac{a_0 - a_1}{\cos\phi} = \sqrt{2}\frac{13}{14}a_0,$$

where $\phi = \pi/4$. Thus, the total travel time along an expanding geodesic satisfies by (2):

$$T = \frac{s}{\sqrt{c^2 + V^2}} = \sqrt{2}\frac{13}{14}\frac{a_0}{\sqrt{2}c} = \frac{13}{14}\frac{a_0}{c} \gtrsim 10 \text{ Gyr}.$$

Example 6. According to Abbott et al. (2020), the total mass after coalescence of two black holes was $150\,M_\odot$ at the luminosity distance 5.3 Gpc. The redshift of the associated event GW190521 is $z \approx 0.82$, which leads to $k = 0$ by Pilipenko (2013). However, by Theorem 1 for $k = 1$ the corresponding comoving distance is about $\theta = 0.6$ for $V = c$ and by (6) the reduction factor $R(\theta) = 1.13$, see Figure 4. Note that in Abbott et al. (2020) nothing is mentioned about the curvature of the universe. Hence, the mass of the resulting black hole calculated from detected gravitational waves could be reduced to $150\,M_\odot/1.13 = 133\,M_\odot$. In Křížek and Somer (2022), we present several other arguments why masses of such calculated black holes are largely overrated. Note that no mechanism is known which would produce binary stellar black holes with masses greater than 50 solar masses. Moreover, there is a large statistically significant mass gap between all known black hole mergers and binary neutron stars, and also between single stellar black holes and binary black hole mergers. Therefore, we should carefully distinguish between an observed and calculated stellar black hole to avoid overestimating its mass and to eliminate those gaps.

Remark. For $V = c$ the equatorial hyperplane of $\mathbb{S}^3_a$ with angle $\theta = \pi/2$ corresponds by (20) to the redshift

$$z = \mathrm{e}^{\pi/2} - 1 = 3.81,$$

see Table 2. The assumption $V = c$ is quite realistic, because of the following inequality

$$V \approx \frac{a(t_0)}{t_0} > \frac{10^{26}}{13.8 \cdot 10^9 \cdot \pi \cdot 10^7} \text{ m/s} = 0.75c,$$

see (2), (8), and (16). If $V \neq c$ then the above relations have to be appropriately modified.

5. Arguments against unbounded manifolds

Let us point out that six different ways to imagine hyperbolic geometries are clearly described in Cannon et al. (1997), see also Brandts at al. (2024) and Křížek (2023, p. 135). According to Blanuša (1955), Křížek and Pradlová (2003), the hyperbolic pseudosphere $\mathbb{H}^3$ cannot be isometrically imbedded to Euclidean space $\mathbb{E}^4$ like $\mathbb{S}^3$ in (1). John Nash (1954) proves that $\mathbb{H}^3$ can be isometrically imbedded to $\mathbb{E}^7$ and it is not known whether the exponent 7 can be reduced. We only know that there exists a local isometric imbedding from $\mathbb{H}^3$ to $\mathbb{E}^5$ (see Brander (2007)). Hence, $\mathbb{H}^3$ is a very unusual and quite exceptional manifold.

The unbounded manifolds $\mathbb{H}^3$ and also $\mathbb{E}^3$ serve as a model of an infinite isotropic and homogeneous universe in the standard ΛCDM cosmology. Nevertheless, the fact that such an infinite universe for a fixed time instant would have at each point almost the same curvature, density, pressure, temperature, etc., on large scales is very unlikely. This would require an infinite speed of information transfer which is impossible. On the other hand, the manifold $\mathbb{S}^3_a$ is always bounded having a finite volume. So if the expansion is slow, then all parts of $\mathbb{S}^3_a$ can mutually influence to guarantee homogeneity and isotropy of early universe. Hence, no inflation epoch is necessary.

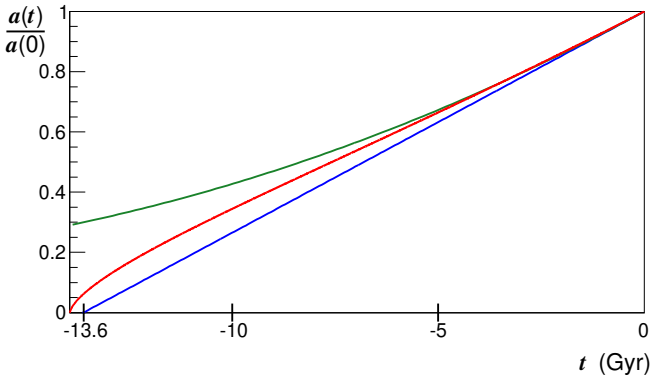

Fig. 7. The middle red graph illustrates the behavior of the normalized expansion function $a(t)/a(0)$ calculated numerically from the Friedmann normalized equation (24) for $k = 1$, $\Omega_{\mathrm{M}} \doteq 0.3$, $\Omega_\Lambda \doteq 0.7$, and $H_0 = 70$ km/(s Mpc). The time variable is shifted for simplicity so that $t_0 = 0$ corresponds to the present time. The lower blue graph corresponds to the linear function $1+H_0t$ on the interval $[-1/H_0, 0]$. The upper green graph shows the quadratic function $1+H_0t-\frac{1}{2}q_0H_0^2t^2$ with deceleration parameter $q_0 = -0.6$. The accelerated expansion differs only very little from the linear expansion during the last few Gyr.

Now let $\rho = \rho(t)$ be the mean mass density of the universe at time t, G be the gravitational constant, and let Λ be the cosmological constant. The standard ΛCDM model is based on the following ordinary differential equation

for the unknown expansion function $a = a(t)$ (see Friedmann (1922, 1924))

$$\dot{a}^2 = \frac{8\pi G\rho a^2}{3} + \frac{\Lambda c^2 a^2}{3} - kc^2. \tag{23}$$

At present it is called the *Friedmann equation* for the curvature index $k \in \{-1, 0, 1\}$. Since the terminal condition (18) for the present time t_0 is known, we may integrate (23) backward in time.

Dividing (23) by $\dot{a}^2$ and using (17), we can easily derive the so-called *normalized Friedmann equation* which is usually written in the form (see e.g. Peebles (1993), Perlmutter at al. (1997), Planck Collaboration (2014))

$$1 = \Omega_{\mathrm{M}} + \Omega_\Lambda + \Omega_k, \tag{24}$$

which is still a differential equation, even though it does not look like that. Here, $\Omega_{\mathrm{M}}(t) = \frac{8}{3}\pi G\rho(t)/H^2(t)$, $\Omega_\Lambda(t) = \frac{1}{3}\Lambda c^2/H^2(t)$, and the measured value of the third *density curvature parameter*

$$\Omega_k(t) = -\frac{kc^2}{\dot{a}^2(t)} \tag{25}$$

is in absolute value extremely small. From this many cosmologists deduce that $k = 0$. However, this is a completely false mathematical implication, since the time derivative $\dot{a}$ can be very large. We will illustrate these facts by several further important examples.

Example 7. By (16) and the Mean Value Theorem of differential calculus there exists $t_3 \in (0, t_2)$ such that $\dot{a}(t_3) > 25\,c$. From this and by inserting $t = t_3$ into (25), (i.e., the Friedmann differential equation (23) becomes algebraic), we find that density curvature parameter can be really very small for $k \neq 0$, namely, we have the following two-sided estimate

$$0 < |\Omega_k(t_3)| = \Big|\frac{kc^2}{\dot{a}^2(t_3)}\Big| < \frac{1}{625}.$$

Hence, the case $k = 1$ is possible for the time instant $t = t_3$. Moreover, from Section 3 we know that the spherical geometry of the universe cannot suddenly jump during its evolution to the Euclidean or hyperbolic geometries.

Example 8. According to Andreon et al. (2023, p. 4302), the mass of the galaxy cluster JKCS 041 with $z = 1.803$ is $4 \cdot 10^{14} M_\odot$. Such a large mass was obtained from measured luminosities for $\Omega_{\mathrm{M}} \doteq 0.3$, $\Omega_\Lambda \doteq 0.7$, and $k = 0$. However, for $k = 1$ the luminosity distance would be somewhat different. Namely, by Theorem 1 the corresponding comoving distance of JKCS 041 is $\theta \approx 1.03$ rad if $V \approx c$. Hence, the above large mass could be reduced approximately 1.44 times, since the reduction factor $R(\theta) \approx 1.44$, see Figure 4. See also Andreon et al. (2021).

Example 9. Kroupa et al. (2020) investigate a very rapid emergence of supermassive black holes with high cosmological redshifts, e.g. when $z = 9.1$

(see also Kovács et al. (2024)). By Theorem 1 the corresponding comoving distance is $\theta = 2.3$ rad for $V \approx c$. This leads to the reduction factor $R(\theta) \approx 10$. Hence, these early black holes are perhaps not so supermassive as assumed when we replace $k = 0$ by $k = 1$. Thus also the mass of a very distant black hole with $z = 7.5$ (see Yang et al. (2020)) is considerably overestimated.

Recently the most distant known blazar J0410-0139 was detected, one of whose jets is directed to us. Blazars are statistically very rate cases of active galactic nuclei. It can be assumed that when we observe a blazar, then at a similar redshift distance $z \approx 7$ there are many more similar objects, but their jets are not pointing in our direction.

Example 10. Baryonic acoustic oscillations (BAO) are fluctuations in the density of the visible baryonic matter caused by acoustic waves of the primordial plasma in the time period (12). According to Eisenstein and Bennett (2008), the power spectrum of CMB indicates that the angular size of the most frequent fluctuations is approximately equal to $\varphi = 1^\circ$ that is $\varphi = 2\pi/360 = 0.01745$ rad, see the right half of the sphere in Figure 1. Now we will estimate its actual diameter D at time t_2 for all three cases $k = 1, 0, -1$ by means of the angular distance (see Křížek and Somer (2023, p. 149) and Weinberg (1972, p. 423)). From (9), (10), and (5) we find that

$$D = \varphi a(t_2)\,\mathrm{sinn}\,\theta,$$

namely,

$$D = \begin{cases} \varphi a(t_2)\sin\theta & \text{if } k = 1, \\ \varphi a(t_2)\theta & \text{if } k = 0, \\ \varphi a(t_2)\sinh\theta & \text{if } k = -1, \end{cases} \tag{26}$$

where by (14),

$$\varphi a(t_2) \gtrsim 0.157 \text{ Mly}. \tag{27}$$

Unfortunately, we cannot apply Theorem 1 to establish more precisely the comoving distance θ of the CMB, since the expansion function is far from being linear near t_2. (By (16) the slope angle would be extremely small: $\phi < 2.29^\circ$ for $c/V < 1/25$.) Anyway, we can use the lower bound (14) and assume that $\theta \approx 3$ rad, i.e., the origin of the CMB is close to the South Pole of the expanding 3-sphere (cf. also Table 2). Note that the corresponding reduction factor is then $R(\theta) \approx 452$, see Figure 4. In this case, the actual diameter D can be bounded from below by (26) and (27) as follows

$$D \gtrsim \begin{cases} 0.022 \text{ Mly} & \text{if } k = 1, \\ 0.471 \text{ Mly} & \text{if } k = 0, \\ 1.574 \text{ Mly} & \text{if } k = -1. \end{cases} \tag{28}$$

We observe that the actual physical size of the most frequent fluctuations is dramatically different for spherical, flat, and hyperbolic universe. Since the period, when CMB had appeared, was only about 10^4 yr, the most probable case is again $k = 1$. The diameter in (28) for $k \le 0$ is so large that it contradicts the causality principle, since acoustic waves could not travel such a long distance due to (12).

Now we present another argument against hyperbolic and Euclidean geometries of the physical universe. A positive curvature of the space arises in the interior of a homogeneous mass ball with radius $R > 0$ and the Schwarzschild radius $S < R$. The corresponding line element in the standard spherical coordinates is given by (see e.g. Ellis (2012), Florides (1974), Stephani (2004))

$$\mathrm{d}l^2 = \frac{1}{1 - r^2 s^2}\,\mathrm{d}r^2 + r^2\mathrm{d}\theta^2 + r^2\sin^2\theta\,\mathrm{d}\varphi^2, \tag{29}$$

where $rs \in [0, 1)$, $s = \sqrt{S/R^3}$, $\theta \in [0, \pi]$, and $\varphi \in [0, 2\pi)$. This equality looks similarly to (see Weinberg (1972, p. 403), Křížek and Somer (2023, p. 118))

$$\mathrm{d}l^2 = \frac{1}{1 - kr^2}\,\mathrm{d}r^2 + r^2\mathrm{d}\theta^2 + r^2\sin^2\theta\,\mathrm{d}\varphi^2 \tag{30}$$

for the FLRW line element of the 3-sphere with the curvature index $k = 1$. Here $r \in [0, 1)$ is a dimensionless parameter, $\theta \in [0, \pi]$, and $\varphi \in [0, 2\pi)$. We observe that the cases $k = 0$ and $k = -1$ do not match (29). Thus, the presence of a homogeneous mass distribution causes a positive curvature globally and the most natural model of the physical universe is $\mathbb{S}^3_a$ for a fixed time instant.

Another argument is based on the hypothesis that no physical quantity (including the diameter of the universe) can attain an infinite value. Several arguments against unbounded manifolds used to describe the physical universe are also given in previous sections.

6. Final remarks

Is the global curvature of the universe positive? In Examples 1, 2, and 3 (see also Figures 1, 2, 5, and 6) we introduced there different magnification effects to show how the spherical geometry magnifies angular sizes leading to the spacetime-lens principle which could explain the large observed flux intensity of galaxies at $z \gtrsim 13$, cf. (22). Therefore, a positive curvature index $k = 1$ allows us to explain why in the early universe we observe:

1) supermassive stars,
2) too large stellar black holes,
3) supermassive black holes,
4) too long jets and their superluminal velocities of distant quasars,
5) too large early galaxies,
6) too large early galaxy superclusters,
7) large size of the most frequent fluctuations in CMB,
8) super energetic quasars,
9) giant γ-ray bursts,
10) very luminous supernovae,...

All these objects, mentioned e.g. in Kroupa et al. (2020), Mészáros (2019), Mészáros et al. (2011), Yang (2020) could only be due to apparent optical effects. Their absolute bolometric luminosities are just smaller than it is supposed.

Moreover, in Section 3, we showed how the time-lens principle magnifies the angular sizes of distant objects. The main theorem that states how to estimate the comoving distance for a given redshift when $k = 1$ is proved in Section 4. In Section 5, we demonstrated why

$$\Omega_{\mathrm{M}} + \Omega_{\Lambda} \doteq 1 \not\Rightarrow k = 0.$$

We also presented several typical examples of phenomena that should be revised from the case $k = 0$ to $k = 1$.

Cosmologists often claim that our universe has no center. Nevertheless, in Figure 5 we observe that the blue manifold has its center on the time axis t even though this center does not belong to $\mathbb{S}^1_a$. (The circle $x^2 + y^2 = 1$ also has a center which does not belong to it.) The observable universe (the yellow manifold in Figure 5) is centered on Earth and the center of spacetime (represented by the red manifold) corresponds to the Big Bang at the origin of the spacetime coordinates.

In the Hubble test of a local homogeneity of the universe, one has to measure the apparent magnitude (energy flux ℓ from a given galaxy). By Carpenter (1938) the number of observed galaxies in the sky brighter than ℓ should vary as $\ell^{-3/2}$, see also Li and Liu (2015), Peebles (1993), Weinberg (1972). This test should be modified for non-Euclidean geometries, in particular for $\mathbb{S}^3_a$. Several other results should be revised from the case $k = 0$ to $k = 1$ as well due to very large differences of numbers in (28).

The fact that we do not observe too many galaxies with $z > 10$ also indicates that $k = 1$ and $\theta \in (\pi/2, \pi)$. Their number is proportional to $\operatorname{sinn}^2\theta$, where sinn is defined in (10). For $k \le 0$ we would observe a large amount of galaxies with $z > 10$ which is not the case. The distribution of distant quasars is also not so dense as predicted in Nguyen et al. (2020).

Acknowledgments. I am deeply grateful to Jan Brandts (Univ. of Amsterdam) and Attila Mészáros (Charles Univ.) for fruitful discussions. This research was funded by the Czech Academy of Sciences (RVO 67985840) and grant no. 24-10586S of the Czech Science Foundation.

References

Abbott B. P. et al., 2020, *Phys. Rev. Lett.* 125, 101102
Andreon S. et al., 2021, *Mon. Not. Roy. Astron. Soc.* 505, 5896–5909
Andreon S. et al., 2023, *Mon. Not. Roy. Astron. Soc.* 522, 4301–4309
Blanuša D., 1955, *Monatsh. Math.* 59, 217–229
Brander D., 2007, *Ann. Global Anal. Geom.* 32, 253–275
Brandts J., Křížek M., Somer L., 2024, *Symmetry* 16, Article 141
Cannon J. W., Floyd W. J., Kenyon R., Parry W. R., 1997, *Hyperbolic geometry.* In: Flavors of Geometry, Math. Sci. Res. Inst. Publ. 31, Cambridge Univ. Press, 59–115
Carpenter E. F., 1938, *Astrophys.* J. 88, 344
Carroll S., 2014, *Spacetime and geometry. An introduction to general relativity*, Pearson, Harlow
Carroll S. M., Press W. H., Turner E. L., 1992, *Annu. Rev. Astron. Astrophys.* 30, 499–542
Chiba T., Nakamura T., 1998, *Prog. Theor. Phys.* 100, 1077–1082
Davis, T. M., Lineweaver C. H., 2004, *Publ. Astron. Soc. Australia* 21, 97–109
Einstein A., 1917, *Königlich-Preuss. Akad. Wiss.*, Berlin, 142–152; English translation in The principle of relativity. New York, Dover, 1952.

Eisenstein D. J., Bennett C. L., 2008, *Physics Today* 61, 44–50
Ellis H. G., 2012, ArXiv: 1203.4750v2.
Florides P. S., 1974, *Proc. Roy. Soc. London A* 337, 529–535
Friedman A., 1922, *Z. Phys.* 10, 377–386; English translation in General Relativity and Gravitation 31 (1999), 1991–2000
Friedmann A., 1924, *Z. Phys.* 21, 326–332; English translation in General Relativity and Gravitation 31 (1999), 2001–2008
Kovács O. E. et al., 2024, *Astrophys. J. Lett.* 965, L21
Křížek M., 1999, *Pokroky Mat. Fyz. Astronom.* 44, 218–226
Křížek M., 2024, *Bulg. Astron. J.* 40, 25–35
Křížek M., Křížek F., Somer L., 2015, *Antigravity — its origin and manifestations*, Lambert Acad. Publ., Saarbrücken
Křížek M., Pradlová J., 2003, *Math. Comput. Simulation* 61, 525–535
Křížek M., Somer L., 2022, *Galaxies* 10, Article 52
Křížek M., Somer L., 2023, *Mathematical aspects of paradoxes in cosmology. Can mathematics explain the contemporary cosmological crisis?*, Springer, Cham
Kroupa P. et al., 2020, *Mon. Not. Roy. Astron. Soc.* 498, 5652–5683
Labbé I. et al., 2023, *Nature* 616, 266–269
Laporte N. et al., 2021, *Mon. Not. R. Astron. Soc.* 505, 3336–3346
Li M.-H., Liu H.-N., 2015, *Astron. Astrophys.* 582, A111
Mészáros A., 2019, *Astron. Nachr.* 340, 564–569
Mészáros A., Řípa J., Ryde F., 2011, *Astron. Astrophys.* 529, A55
Nash J., 1954, *Ann. of Math.* 60, 383–396
Nguyen N. H. et al., 2020, *Astrophys.* J. 895, 74
Pearson T. J., Zensus J. A. (eds.), 1987, *Superluminal radio sources*, Cambridge Univ. Press
Peebles P. J. E., 1993, *Principles of physical cosmology*, Princeton Univ. Press, New Jersey
Penrose R., 2005, *The road to reality*, Vintage Books, London
Perlmutter S. et al., 1997, *Astrophys. J.* 483, 565–581
Pilipenko S. V., 2013, ArXiv: 1303.5961v1, 1–4
Planck Collaboration, 2014, *Astron. Astrophys.* 571, A16
Schwarzschild K., 1900, *Vierteljahrsschift der Astronomischen Gesellschaft* 35, 337–347; English translation in Abraham Zelmanov J. 1 (2008), 64–73
Stephani H., 2004, *Relativity: An introduction to special and general relativity*, 3rd edition, Cambridge Univ. Press, Cambridge
Suntola T., 2018, *The dynamic universe, toward a unified picture of physical reality*, 4th edition, Physics Foundations Society, The Finnish Society for Natural Philosophy
Vavryčuk V., 2018, *Mon. Not. Roy. Astron. Soc.* 478, 283–301
Wang B. et al., 2023, *Astrophys. J. Lett.* 957, L34
Weinberg S., 1972, *Gravitation and cosmology: Principles and applications of the General Theory of Relativity*, John Willey & Sons, Inc., New York
Yang J. et al., 2020, *Astrophys. J. Lett.* 897, L14